Re-examination of Small-Signal Instability in Weak Grid-Connected Voltage Source Converters

Tao Xue, Ulas Karaagac, Haoyan Xue, and Jean Mahseredjian

***Abstract*-- Weak grid sub-synchronous oscillation (SSO) is an important research topic. Although some analysis and mitigation schemes have been conducted, misperceptions still exist. This paper first aims to update the understanding of weak grid instability of voltage source converters (VSCs) and then points out that instability risks originate in the super-synchronous frequency range rather than in the sub-synchronous frequency range. Moreover, the resonance frequency can be even larger than the double fundamental frequency under certain parameter conditions. This paper also refines the impacts of VSC control parameters on weak grid instability mechanism and resonance frequency. Based on the results, the classification of this phenomenon should be revised.**

***Keywords*: Weak grid instability, VSC, stability analysis.**

I. Introduction

THE interaction between voltage source converter (VSC) and weak (low short circuit ratio, low SCR) AC grid is called weak grid sub-synchronous oscillation (SSO) [1], which belongs to a new type of stability issue: converter-driven stability [2]. Weak grid SSO has been confirmed in several real-world incidents [3]. Those events occurred in weak grid-connected wind parks (WPs) or photovoltaic (PV) farms without series compensation. In Texas, 4 Hz oscillations were observed at a type-4 WP after a transmission line tripped [4]. The WP was integrated into the grid with two transmission lines initially but then experienced a weak grid condition after one line was taken out of service. In west China, 30 Hz oscillations occurred in 2015 when type-4 WPs raised output active power [5]. The WPs in west China were connected to the main grid with long transmission lines, which created a weak grid condition. Other weak grid SSO events caused by interactions between grid-connected VSC and weak grid include 2.5 Hz oscillations in Hydro One's type-4 WP [6], 9 Hz oscillations in an offshore WP of Great Britain [7], 8 Hz oscillations in WPs of Scotland [8], 7 Hz oscillations caused by inverter-based resources (IBRs) in West Murray Zone of Australia [9], 22 Hz oscillations in PV farm of Dominion Energy in the eastern U.S [10], 20 Hz oscillations in Hydro One's PV farm [11], 7 Hz oscillations in First Solar's California PV farm [12].

The weak grid SSO mechanism is initially explained as a power transfer issue by circuit analysis [13]. When the reference of VSC output active power increases, the output currents also increase, leading to a larger voltage drop on equivalent grid impedance, so active power decreases. Instability occurs because of the imbalance between the VSC output active power and controller reference. Based on this mechanism, the damping controller is designed to weaken the couplings between active power and the output voltage [14]. On the other hand, the VSC controls also have significant impacts on the weak grid SSO. Initially, the phase-locked loop (PLL) parameters are found as the major reason in Texas and west China events and modifying PLL parameters is recommended for mitigation in [15]. Then impedance-based stability analysis (IBSA) brings new insights to the weak grid SSO issue **Error! Reference source not found.**. The IBSA explains the instability as a resonance circuit formed by the VSC and the weak grid, and it can be displayed in the R-X diagram analysis [17], [18] or Bode diagram analysis [19]. The impacts of other control parameters of the inner and outer control loops, decoupling, and voltage feedforward terms on the impedance characteristics of VSC are analyzed in [20].

Among some literature on real-world events and weak grid SSO analysis, the VSC phase current and voltage spectrums contain components not only at fundamental and resonance frequencies (f_b and f_r), but also at mirror frequency ($f_m = 2f_b - f_r$) [3]. This phenomenon is defined as Mirror Frequency Effect (MFE) when some researchers are studying the relations of different impedance models [21]. But it is initially ignored in the analysis of real-world events because it cannot be detected by RMS measurements or simulations [3]. The RMS measurements only show the frequency differences between f_r and f_b, and also between f_m and f_b, i.e. $|f_r - f_b| = |f_m - f_b| = f_{RMS}$. In the Dominion Energy event [10], 22 Hz oscillations were observed in RMS measurements. However, Power Spectral Density (PSD) plots on Point on Wave (PoW) data of both phase voltages and currents showed an 82 Hz (60 Hz + 22 Hz) component along with a 38 Hz (60 Hz − 22 Hz) component [3]. This is not a coincidence or a specific case. In the Hydro One event [11], a 20 Hz component was found in the RMS measurement of voltages, while an 80 Hz (60 Hz + 20 Hz) component was found in the Fast Fourier Transformation (FFT) spectrum of the phase currents. But no further information about whether the 40 Hz (60 Hz − 20 Hz) component exists. Some researchers noticed this issue but had not investigated further. The study in [20] shows two frequency components at 20 Hz (50 Hz − 30 Hz) and 80 Hz (50 Hz + 30 Hz) when analyzing the 30 Hz West China event [5], but it lacks

This work was supported by the Hong Kong Research Grant Council for the Research Project under Grant 25223118.

T. Xue and U. Karaagac, are with the Department of Electrical Engineering, Hong Kong Polytechnic University, Hung Hom, Kowloon, Hong Kong.

Haoyan Xue and J. Mahseredjian are with the Department of Electrical Engineering, Polytechnique Montréal, Montreal, QC, Canada.

Paper submitted to the International Conference on Power Systems Transients (IPST2023) in Thessaloniki, Greece, June 12-15, 2023.

the analysis to identify the resonance.

This confusion remains unsolved as the weak grid-connected VSC instability is defined as weak grid SSO due to the observations of sub-synchronous component either in the RMS or phase voltage/current measurements. However, FFT spectrum of phase voltage/current measurements also contains super-synchronous component, so it should be further investigated to decide which component is the initiator (resonance frequency component) and which is the responder (mirror frequency component). Classifying weak grid-connected VSC instability as weak grid SSO leads to the misperception that the sub-synchronous component is the initiator, which is incorrect in most cases. This classification may cause further confusion when the resonance frequency is larger than the double fundamental frequency (i.e., $f_r > 2f_b$).

This paper aims to study the instability mechanism on a typical weak grid test system through IBSA and demonstrate instability in the super-synchronous frequency range so that the confusion can be explained. The IBSA results are also validated through electromagnetic transient (EMT) simulations. As the resonance frequency is in the super-synchronous frequency range, the classification of weak grid-connected VSC instability should be revised.

The rest of this paper is arranged as follows. Section II presents the test system and its impedance model, briefly. The weak grid-connected VSC instability mechanism is explained in Section III. Section IV refines the impact of VSC control parameters on weak grid instability. Section V presents illustrative examples and EMT validation. Finally, Section VI concludes the paper.

II. Test System and IBSA Model

The test system is shown in Fig. 1, where a grid-tied VSC (can represent type-4 WPs, solar farms, etc.) is connected to an infinite bus through two parallel impedances ($Z_1 // Z_2$).

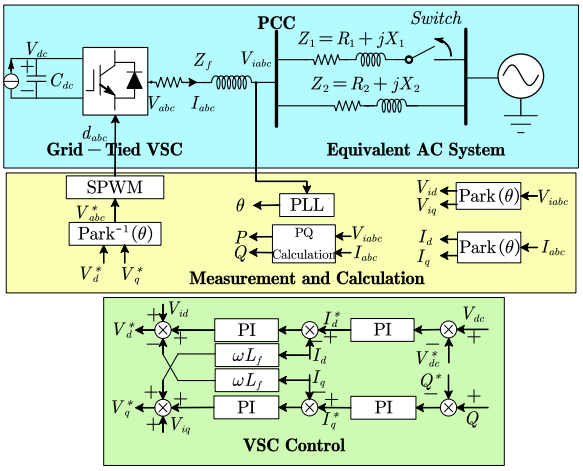

Fig. 1 Circuits, controls, and configurations of the test system

The VSC uses DC voltage control at d-axis outer loop and reactive power control at q-axis outer loop. The inner loop uses current vector control. Park transformation and its inverse are conducted on the angle provided by PLL. The AC system equivalent impedance is modified by disconnecting impedance Z_1 (only Z_2 is connected, so Z_{grid} refers to Z_2 thereafter) to obtain the weak grid connection scenario. The system parameters are given in TABLE V of the appendix.

This paper uses IBSA to explain the instability mechanism. VSC impedance model is well established in [22], and the final equation in the dq domain is

$$\mathbf{Z_{vscdq}} = \left\{\mathbf{A}^{-1}\left[\mathbf{B} - \mathbf{C}(sC_{dc} + F + H)^{-1}\mathbf{G}\right]\right\}^{-1} \tag{1}$$

The grid is represented by voltage behind impedance, and its dq domain impedance model is

$$\mathbf{Z_{griddq}} = \begin{bmatrix} R_{grid} + sL_{grid} & -\omega_b L_{grid} \\ \omega_b L_{grid} & R_{grid} + sL_{grid} \end{bmatrix} \tag{2}$$

Detailed explanations of the matrices of (1) can be found in [22]. ω_b in (2) is the fundamental frequency. The dq domain multi-input multi-output (MIMO) impedances can be transformed into the sequence domain single-input single-output (SISO) impedances by the transformation given in [20]. This process includes a linear transformation and a model simplification. The linear transformation turns dq domain MIMO impedances into modified sequence MIMO impedance:

$$\begin{aligned} &\begin{bmatrix} Z_{pp}(s) & Z_{pn}(s) \\ Z_{np}(s) & Z_{nn}(s) \end{bmatrix} = \frac{1}{2}\begin{bmatrix} 1 & j \\ 1 & -j \end{bmatrix}\begin{bmatrix} Z_{dd}(s) & Z_{dq}(s) \\ Z_{qd}(s) & Z_{qq}(s) \end{bmatrix}\begin{bmatrix} 1 & 1 \\ -j & j \end{bmatrix} \\ &\Rightarrow \mathbf{Z_{pn}}(s) = \frac{1}{2}\begin{bmatrix} 1 & j \\ 1 & -j \end{bmatrix}\mathbf{Z_{dq}}(s)\begin{bmatrix} 1 & 1 \\ -j & j \end{bmatrix} \end{aligned} \tag{3}$$

Then the model simplification turns modified sequence MIMO impedances into the sequence domain SISO impedances:

$$Z_p(s) = \frac{\det\left[\mathbf{Z_{pn}}(s - j\omega_b)\right]}{Z_{nn}(s - j\omega_b)} \quad Z_n(s) = \frac{\det\left[\mathbf{Z_{pn}}(s + j\omega_b)\right]}{Z_{pp}(s - j\omega_b)} \tag{4}$$

The R-X diagram is used to explain the instability mechanism. The Bode diagram is omitted but the results are used to provide the intersection frequencies and phase margins in the following sections. In the R-X diagram, instability occurs when the product of resistance and derivative of reactance is negative at reactance cross-over frequency f_0 **Error! Reference source not found.**:

$$\left(R_{sys} \cdot \frac{dX_{sys}}{df}\right)\Big|_{f_0} < 0 \tag{5}$$

where

$$\begin{aligned} Z_{sys}(f) &= R_{sys}(f) + jX_{sys}(f) \\ &= \left[R_{vsc}(f) + R_{grid}(f)\right] + j\left[X_{vsc}(f) + X_{grid}(f)\right] \end{aligned} \tag{6}$$

In the Bode diagram, instability occurs when the absolute value of the phase difference is larger than 180° at the intersection frequency f_d of the VSC and grid impedance magnitude curves [19]:

$$\begin{cases} \left|Z_{vsc}(f_d)\right| = \left|Z_{grid}(f_d)\right| \\ \left|\angle Z_{vsc}(f_d) - \angle Z_{grid}(f_d)\right| > 180° \end{cases} \tag{7}$$

The reactance cross-over frequency f_0 is sometimes different from the intersection frequency f_d. The frequency

f_0 reflects natural frequency (LC resonance without considering R), while the frequency f_d reflects damped (or undamped) natural frequency (considering R). f_d is the same as the resonance frequency f_r observed in oscillatory waveforms, and natural frequency f_0 can be used to approximate f_d. However, when the resistance of the system is prominent, the difference between f_0 and f_d increases.

III. Mechanism Analysis of Weak Grid-Connected VSC Instability

A. Impedance Response of the VSC

The VSC impedance response in 1 Hz - 1000Hz is shown in Fig. 2. The characteristics of the VSC vary in different frequency ranges. Those frequency ranges may change under different parameter conditions, and this paper only provides an example and shows the general trend.

In 0 Hz - 40 Hz, VSC impedance is inductive with negative resistance, which has little possibility of interacting with an inductive AC grid and leads to SSO. In 40 Hz - 50 Hz and 50 Hz - 60 Hz (near fundamental frequency), VSC becomes capacitive and inductive with positive resistances, respectively. Although VSC in 40 Hz - 50 Hz can interact with an inductive AC grid, whether the system can be unstable with such a large positive resistance of VSC remains unknown.

VSC impedance is capacitive with negative resistance in 60 Hz - 100 Hz and positive resistance in 100 - 200 Hz. Therefore, VSC can interact with an inductive AC grid in the super-synchronous range, which is the cause of weak grid instability. Moreover, the negative resistance range may expand to 100 Hz - 200 Hz when the bandwidth of the current PI regulator increases and thus shift the instability risk above the double fundamental frequency, which will be discussed in section IV and V. Above 200 Hz, VSC keeps inductive with positive resistance.

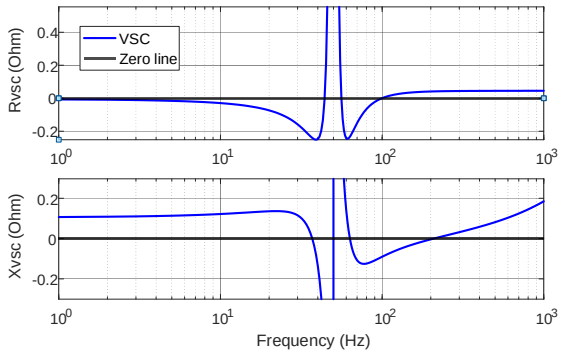

Fig. 2 Impedance response of the VSC.

B. Instability Mechanism Analysis

The impedance responses of the system for various SCRs are illustrated in Fig. 3. AC grid impedance (Z_{grid}) increases with a constant R_{grid} / X_{grid} ratio, and the VSC impedance (Z_{vsc}) remains the same.

In the R-X diagram of Fig. 3, there are three frequency ranges in which reactance crosses over the zero line. The two ranges near the fundamental frequency are safe because the products of resistance and derivative of reactance are positive and will not lead to instability. Only when the Z_{grid} increases to 3pu (almost unreasonable in a real-world power system), the product at the reactance cross-over frequency in the sub-synchronous range has the possibility of becoming a negative value (the cyan line). However, this negative product will be made by a positive resistance and a negative derivative of reactance. This instability (40 Hz - 50 Hz) only exists in a theoretical perspective and not expected in the real power system. Hence, it does not fall into the main topic of this paper.

On the other hand, the reactance cross-over frequency in the third range (50 Hz - 200 Hz) decreases as the Z_{grid} increases, and the resistance becomes negative when the Z_{grid} equals 0.5pu. This negative product is made by a negative resistance and a positive derivative of reactance, which is the expected case in the real power system. Therefore, weak grid instability can occur in the super-synchronous range (50 Hz - 100 Hz) or even above double fundamental frequency (>100 Hz) rather than in the sub-synchronous range (0 Hz - 50 Hz). The classification of SSO is not proper, as the super-synchronous frequency component is the initiator, and the sub-synchronous frequency component is the responder (mirror frequency).

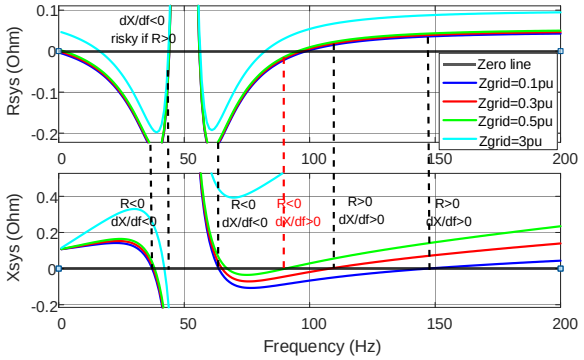

Fig. 3 Impedance responses of the system for various SCRs

IV. Impacts of Control Parameters on VSC Weak Grid Instability

A. Impact of Current PI Regulator

With the increase of current PI regulator bandwidth, the VSC impedance becomes more capacitive in a wide super-synchronous frequency range as shown in Fig. 4. The grid inductive reactance offsets the VSC capacitive reactance at higher frequencies.

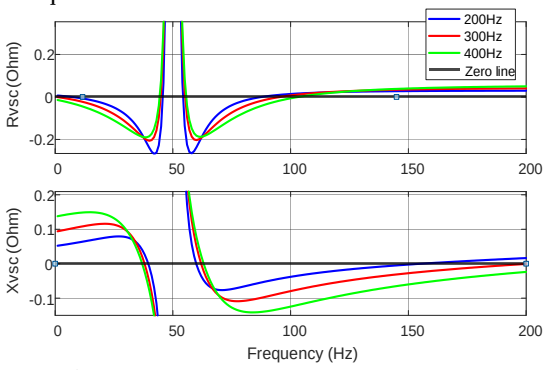

Fig. 4 Impact of VSC current PI regulator bandwidth on impedance responses

of the VSC.

As a result, the reactance cross-over frequency increases significantly as shown in Fig. 5. Although this change causes a decrease in VSC resistance, the system equivalent resistance at the reactance cross-over frequency increases due to the large increase of the reactance cross-over frequency. Hence, the system stability improves. This can be clearly seen from the improvement of the system phase margin presented in Table I.

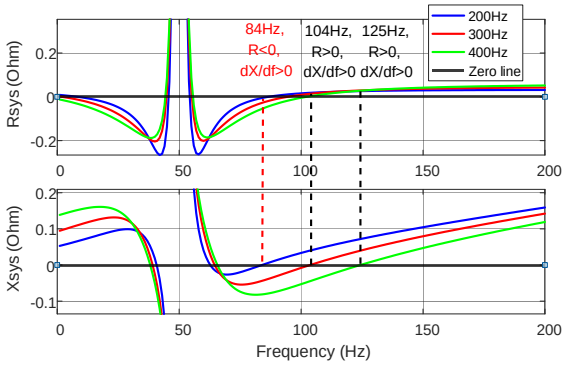

Fig. 5 Impact of VSC current PI regulator bandwidth on impedance responses of the system (R-X diagram stability analysis).

TABLE I
IMPACT OF VSC CURRENT PI REGULATOR BANDWIDTH ON IMPEDANCE RESPONSES OF THE SYSTEM (BODE PLOT STABILITY ANALYSIS RESULTS)

Bandwidth of Current PI Regulator (Hz)	Intersection Frequency (Hz)	Phase Margin (°)
200	84	-5
300	104	10
400	125	19

B. *Impact of PLL*

With the increase of PLL PI regulator bandwidth, the VSC impedance also becomes more capacitive, but in a much narrower super-synchronous frequency range compared to the current PI regulator as seen in Fig. 6. As a result, the reactance cross-over frequency remains unchanged as shown in Fig. 7. The increase of PLL PI regulator bandwidth also causes a significant decrease in VSC resistance and leads to a significant decrease of the phase margin. Hence, the stability is worsened as demonstrated in Table II. The large magnitude of system equivalent resistance results significant deviation of intersection frequencies from the reactance cross-over frequencies obtained through R-X diagram analysis.

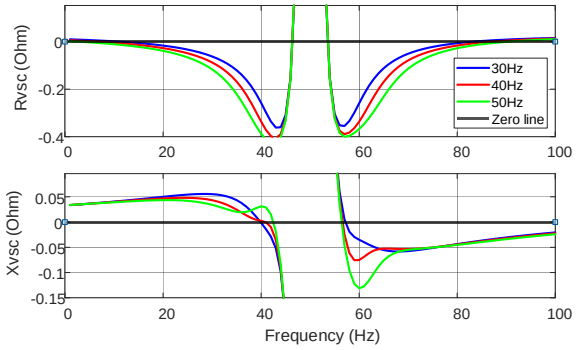

Fig. 6 Impact of VSC PLL PI regulator bandwidth on impedance responses of the VSC.

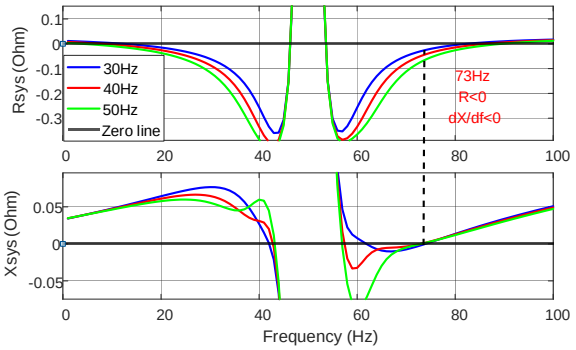

Fig. 7 Impact of VSC PLL PI regulator bandwidth on impedance responses of the system (R-X diagram stability analysis).

TABLE II
IMPACT OF VSC PLL PI REGULATOR BANDWIDTH ON IMPEDANCE RESPONSES OF THE SYSTEM (BODE PLOT STABILITY ANALYSIS RESULTS)

Bandwidth of PLL PI Regulator (Hz)	Intersection Frequency (Hz)	Phase Margin (°)
30	76	-18
40	77	-28
50	79	-33

C. *Impact of DC Voltage PI Regulator*

With the increase of DC voltage PI regulator bandwidth, the VSC impedance mainly changes near the fundamental frequency (40 Hz - 60 Hz) as displayed in Fig. 8. The reactance cross-over frequency remains nearly unchanged and the equivalent system resistance slightly decreases as shown in Fig. 9. As a result, there is a marginal decrease in phase margin as seen in Table III.

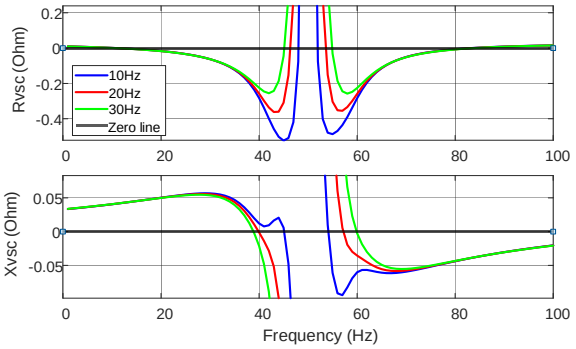

Fig. 8 Impact of VSC DC voltage PI regulator bandwidth on impedance responses of the VSC.

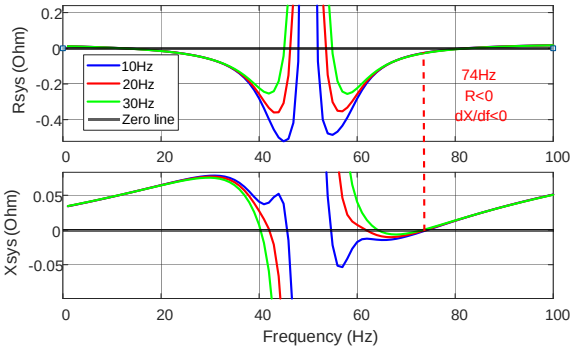

Fig. 9 Impact of VSC DC voltage PI regulator bandwidth on impedance responses of the system (R-X diagram stability analysis).

TABLE III
IMPACT OF VSC DC VOLTAGE PI REGULATOR BANDWIDTH ON IMPEDANCE RESPONSES OF THE SYSTEM (BODE PLOT STABILITY ANALYSIS RESULTS)

Bandwidth of DC voltage PI Regulator (Hz)	Intersection Frequency (Hz)	Phase Margin (°)
10	76	-17
20	76	-18
30	76	-19

D. Impact of Reactive Power PI Regulator

With the increase of the reactive power PI regulator bandwidth, the VSC impedance becomes more capacitive in the super-synchronous frequency range as seen in Fig. 10. As a result, the reactance cross-over frequency slightly increases as shown in Fig. 11. This change also causes a decrease in VSC resistance, and leads to a decrease of phase margin as demonstrated in TABLE IV.

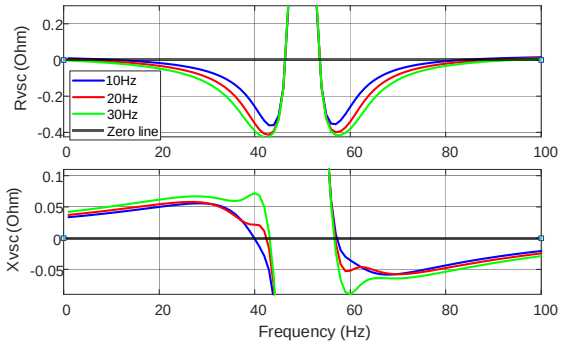

Fig. 10 Impact of VSC reactive power PI regulator bandwidth on impedance responses of the VSC.

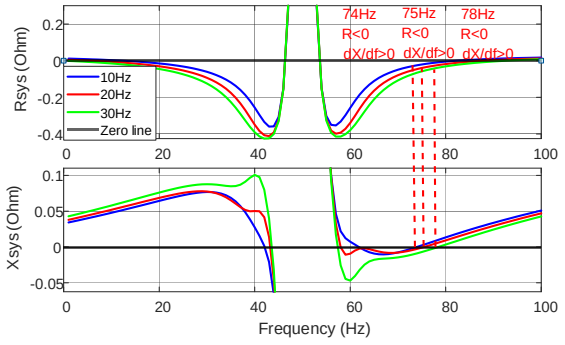

Fig. 11 Impact of VSC reactive power PI regulator on impedance responses of the system (R-X diagram stability analysis).

TABLE IV
IMPACT OF VSC REACTIVE POWER PI REGULATOR BANDWIDTH ON IMPEDANCE RESPONSES OF THE SYSTEM (BODE PLOT STABILITY ANALYSIS RESULTS)

Bandwidth of Reactive Power PI Regulator (Hz)	Intersection Frequency (Hz)	Phase Margin (°)
10	76	-18
20	78	-26
30	81	-27

V. ILLUSTRATIVE EXAMPLES

A. VSC Weak Grid Instability in Super-Synchronous Range

The parameters of the considered test cases are presented in TABLE V. In test case C1, the R-X plot shown in Fig. 12 indicates an instability at 78 Hz as the product of the resistance and the derivative of reactance is negative. There are two more reactance cross-overs at 42 Hz and 60 Hz, but the products of resistance and derivative of reactance are positive. Hence, the system is stable at those two frequencies. From the Bode diagram, the associated phase margin is found as -9.4°. The IBSA is also confirmed by EMT [23] simulations shown in Fig. 13(a) and (b). In the simulation, the switch is opened at t = 1s to reduce the SCR at PCC (see Fig. 1). VSC is represented with its average value model (AVM) [24]. The simulation time step is 50 µs. The FFT analysis presented in Fig. 13(d) shows two frequencies (21.4 Hz and 78.6 Hz) in the current waveform in addition to the fundamental. 78.6 Hz is the resonance frequency and is larger than its 21.4 Hz mirror frequency.

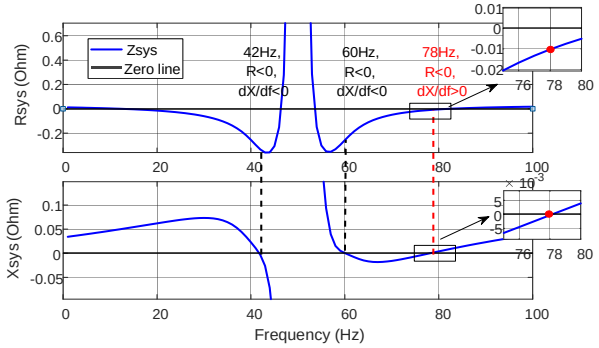

Fig. 12 Impedance response of the system in case C1 (R-X diagram stability analysis).

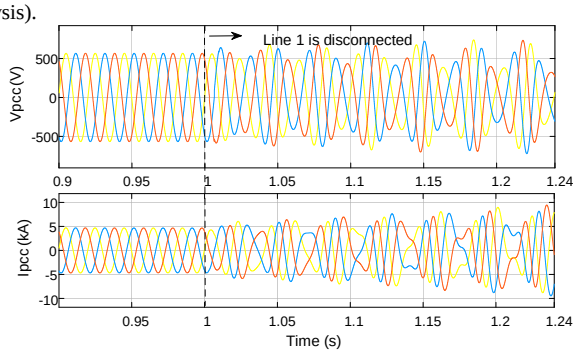

(a)

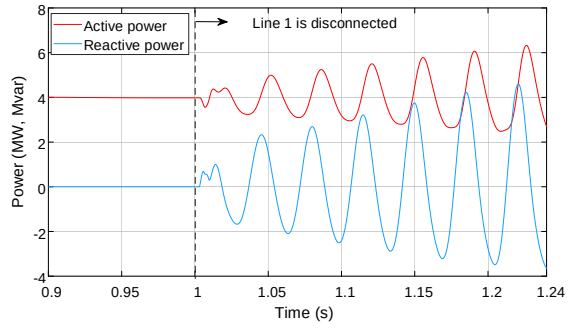

(b)

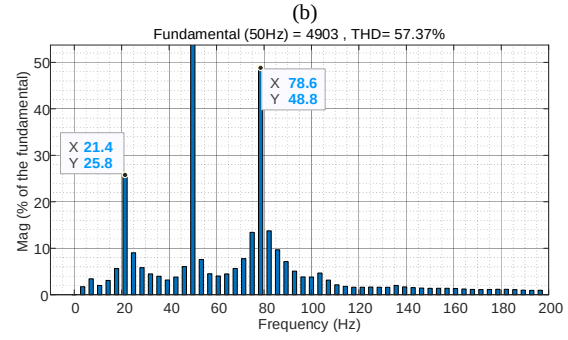

(c)

Fig. 13 EMT simulations of Case C1: (a) three phase voltages and currents, (b) active and reactive power, (c) FFT analysis of the distorted current waveforms.

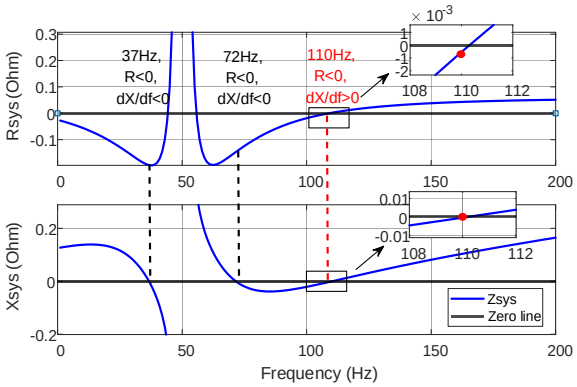

Fig. 14 Impedance response of the system in case C2 (R-X diagram stability analysis).

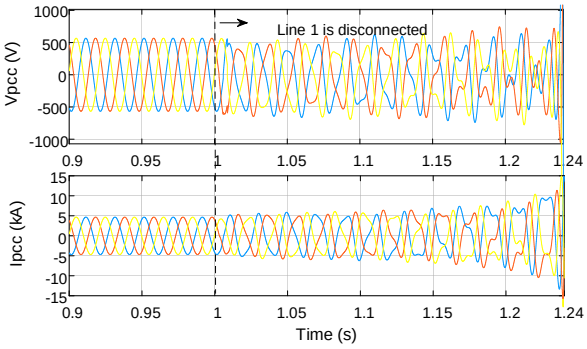

(a)

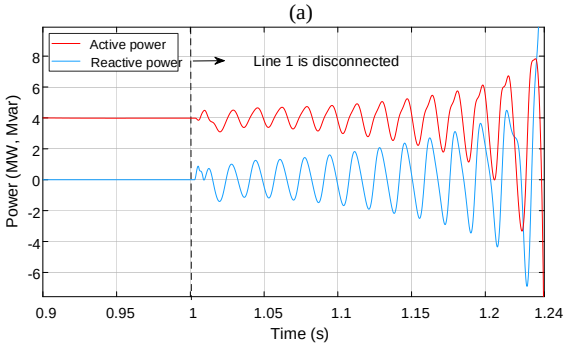

(b)

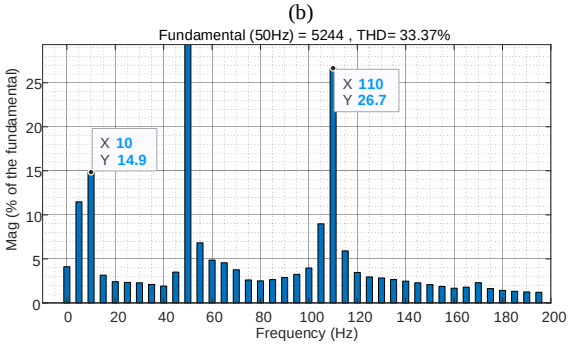

(c)

Fig. 15 EMT simulations of Case C2: (a) three phase voltages and currents, (b) active and reactive power, (c) FFT analysis of the distorted current waveforms.

B. VSC Weak Grid Instability Above Double Fundamental Frequency

In test case C2, the VSC current control and PLL bandwidths are changed from 200 Hz to 400 Hz, and 30 Hz to 45 Hz, respectively. In addition, the low SCR scenario grid impedance Z_2 is increased by 60% (see TABLE V for details). As seen in Fig. 14, those changes shifted the resonance frequency to 110 Hz. The phase margin is -0.3° from the Bode diagram. EMT simulation results presented in Fig. 15(a) and (b) confirm the IBSA. The FFT analysis in Fig. 15(c) shows two frequencies (10 Hz and 110 Hz) in addition to the fundamental. The 10Hz in the FFT spectrum is -10 Hz (= 100 Hz – 110 Hz) in reality. As the resonance frequency is higher than the double fundamental frequency, the mirror frequency becomes negative (i.e., the phase sequence of the oscillation is at opposite).

VI. Conclusions

This paper presented an in-depth analysis of weak grid-connected VSC instability. The IBSA of a typical VSC demonstrated that the instability occurs in the super-synchronous range rather than sub-synchronous. The resonance may occur even above the double fundamental frequency under certain parameter conditions. In this situation, this mirror frequency becomes negative but appears with its positive absolute value in the FFT spectrum. This finding was also confirmed through EMT simulations. In addition, this paper refines the impacts of VSC control parameters on weak grid instability mechanism and resonance frequency.

Classifying weak grid instability phenomenon as weak grid SSO due to the presence of sub-synchronous frequency component causes misperceptions. Hence, its classification should be revised.

VII. Appendix

TABLE V
Parameters of the System

Parameters	Value (Test cases C1 & C2)	
VSC		
Rated DC and ac voltage (V_{dc} , V_{rms})	1130V, 690V	
Rated power (S)	4MW	
L-type filter parameters (R_f , L_f)	0.006Ω, 37.887mH	
DC capacitor (C_{dc})	32.64mF	
Current PI regulator (K_p & K_i)	0.16 & 52.9	0.44 & 375.8
PLL Loop filter (PI regulator) (K_p & K_i)	130 & 8388	194 & 18872
DC voltage PI regulator (K_p & K_i)	0.45 & 19.31	
Reactive power PI regulator (K_p & K_i)	0.05 & 65.97	
Grid impedance (per unit on 4MVA base)		
$Z_1 = R_1 + jX_1$	0.015 + j0.1	
$Z_2 = R_2 + jX_2$	0.015 + j0.25	0.024 + j0.4

VIII. Acknowledgment

This work was supported by the Hong Kong Research Grant Council for the Research Project under Grant 25223118.

IX. References

[1] IEEE PES WindSSO Taskforce, "PES TR-80: Wind Energy Systems Subsynchronous Oscillations: Events and Modeling," 2020.

[2] N. Hatziargyriou *et al.*, "Definition and Classification of Power System Stability - Revisited & Extended," *IEEE Trans. Power Syst.*, vol. 36, no. 4, pp. 3271–3281, Jul. 2021.

[3] Y. Cheng *et al.*, "Real-World Subsynchronous Oscillation Events in Power Grids with High Penetrations of Inverter-Based Resources," *IEEE Trans. Power Syst.*, (early access), pp. 1–15, 2022.

[4] Shun-Hsien Huang, J. Schmall, J. Conto, J. Adams, Yang Zhang, and C. Carter, "Voltage control challenges on weak grids with high penetration of wind generation: ERCOT experience," in *2012 IEEE Power and Energy Society General Meeting*, Jul. 2012, pp. 1–7.

[5] H. Liu *et al.*, "Subsynchronous Interaction Between Direct-Drive PMSG Based Wind Farms and Weak AC Networks," *IEEE Trans. Power Syst.*, vol. 32, no. 6, pp. 4708–4720, Nov. 2017.

[6] C. Li and R. Reinmuller, "Asset Condition Anomaly Detections by Using Power Quality Data Analytics," in *2019 IEEE Power & Energy Society General Meeting (PESGM)*, Aug. 2019, pp. 1–5.

[7] National Grid ESO, "Technical Report on the events of 9 August 2019," 2019.

[8] Julian Leslie, "G-PST/ESIG Webinar Series: Managing Grid Stability in a High IBR Network," *https://www.esig.energy/event/webinar-managing-grid-stability-in-a-high-ibr-network/*, Jan. 2022.

[9] B Badrzadeh, N Modi, C Nathan, and A Jalali, "Power system operation with reduced system strength for inverter-connected generation during prior outage conditions," *CIGRE SCIENCE & ENGINEERING JOURNAL*, vol. 17, pp. 141–149, Feb. 2020.

[10] Dominion Energy, "Identifying Oscillations Injected by Inverter-Based Solar Energy Sources in Dominion Energy's Service Territory using Synchrophasor Data and Point-on-Wave Data," Apr. 2021.

[11] C. Li, "Unstable Operation of Photovoltaic Inverter from Field Experiences," *IEEE Trans. Power Deliv.*, vol. 33, no. 2, pp. 1013–1015, Apr. 2018.

[12] First Solar, "Deploying Utility-Scale PV Power Plants in Weak Grids," Jun. 2017.

[13] L. Fan and Z. Miao, "An explanation of oscillations due to wind power plants weak grid interconnection," *IEEE Trans. Sustain. Energy*, vol. 9, no. 1, pp. 488–490, Jan. 2018.

[14] Y. Li, L. Fan, and Z. Miao, "Stability Control for Wind in Weak Grids," *IEEE Trans Sustain Energy*, vol. 10, no. 4, pp. 2094–2103, Oct. 2019

[15] L. Fan and Z. Miao, "Wind in Weak Grids: 4 Hz or 30 Hz Oscillations?," *IEEE Trans. Power Syst.*, vol. 33, no. 5, pp. 5803–5804, Sept. 2018.

[16] Y. Cheng, M. Sahni, D. Muthumuni and B. Badrzadeh, "Reactance Scan Crossover-Based Approach for Investigating SSCI Concerns for DFIG-Based Wind Turbines," in *IEEE Trans. Power Deliv.*, vol. 28, no. 2, pp. 742-751, Apr. 2013.

[17] U. Karaagac, J. Mahseredjian, S. Jensen, R. Gagnon, M. Fecteau, and I. Kocar, "Safe Operation of DFIG-Based Wind Parks in Series-Compensated Systems," *IEEE Trans. Power Deliv.*, vol. 33, no. 2, pp. 709–718, Apr. 2018.

[18] Y. Cheng, M. Sahni, D. Muthumuni, and B. Badrzadeh, "Reactance scan crossover-based approach for investigating SSCI concerns for DFIG-based wind turbines," *IEEE Trans. Power Deliv.*, vol. 28, no. 2, pp. 742–751, Apr. 2013.

[19] J. Sun, "Impedance-Based Stability Criterion for Grid-Connected Inverters," *IEEE Trans Power Electron*, vol. 26, no. 11, pp. 3075–3078, Nov. 2011.

[20] H. Liu and X. Xie, "Comparative Studies on the Impedance Models of VSC-Based Renewable Generators for SSI Stability Analysis," *IEEE Trans. Energy Convers.*, vol. 34, no. 3, pp. 1442–1453, Sept. 2019.

[21] A. Rygg, M. Molinas, C. Zhang, and X. Cai, "A Modified Sequence-Domain Impedance Definition and Its Equivalence to the dq-Domain Impedance Definition for the Stability Analysis of AC Power Electronic Systems," *IEEE J. Emerg. Sel. Topics Power Electron.*, vol. 4, no. 4, pp. 1383–1396, Dec. 2016.

[22] T. Xue, J. Lyu, H. Wang, and X. Cai, "A Complete Impedance Model of a PMSG-Based Wind Energy Conversion System and Its Effect on the Stability Analysis of MMC-HVDC Connected Offshore Wind Farms," *IEEE Trans. Energy Convers.*, vol. 36, no. 4, pp. 3449–3461, Dec. 2021.

[23] J. Mahseredjian, S. Dennetière, L. Dubé, B. Khodabakhchian and L. Gérin-Lajoie, "On a new approach for the simulation of transients in power systems," *Electric Power Systems Research*, vol. 77, no. 11, pp. 1514-1520, 2007.

[24] S. R. Sanders, J. M. Noworolski, X. Z. Liu, and G. C. Verghese, "Generalized Averaging Method for Power Conversion Circuits," *IEEE Trans. Power Electron.*, vol. 6, no. 2, pp. 251–259, April. 1991.